Gas Processing Journal

Vol. 10, No. 1, 2022, pp. 95 - 112
http://gpj.ui.ac.ir

Research Paper

Simulation of Dehydration Unit with a Pre-cooler to Improve the Hydrate Formation Temperature of Natural Gas

Hadi Amidzadeh[1], Ebrahim Nemati Lay [*,1], Alireza Mohebbi [2], Erfan Kamali [3]

[1] Department of Chemical Engineering, Faculty of Engineering, University of Kashan, Kashan, Iran
[2] Department of Chemical Engineering, School of Chemical and Petroleum Engineering, Shiraz University, Shiraz, Iran
[3] Department of Mechanical Engineering, Islamic Azad University, Dariun Branch, Dariun, Iran

Received: 2022-05-26 Revised: 2022-10-14 Accepted: 2022-11-27

Abstract: The presence of water vapor in natural gas can cause several problems such as corrosion in transmission pipelines, blockage of equipment, and reduction of pipeline capacity. Dehydration is a critical step to reduce the water content to prevent these serious drawbacks. The adsorption process is one of the efficient technologies for producing natural gas with low water content. In this study, the industrial molecular sieve-based dehydration unit is simulated. After validating the simulation results with the plant data, the effect of feed gas cooling before entering the dehydrator on the hydrate formation temperature of the produced dry gas is investigated. To do so, we simulate the dehydration unit with a pre-cooler and design the heat exchanger to reduce the feed gas temperature. In addition, we investigate the effect of temperature reduction on the temperature of hydrate formation and water content for dry gas products. On the other hand, the effect of heating time in the regeneration step on the unit performance is discussed. Because of sufficient cooling operation, the temperature of hydrate formation reduces significantly. For the reduction of 15℃ in the feed temperature, about 50% reduction in the product water content is attained. As a result, the improvement of 6 to 7˚C in the temperature of hydrate formation is achieved for the proposed dehydration process with the pre-cooler in comparison with a simple dehydrator scheme depending on pressure. For the proposed heating time of 8000s, the rise of 6.8% in the total amount of the removed water is achieved.

keywords: Adsorption, Dehydration, Molecular sieve, Natural gas, Simulation.

1. Introduction

1.1. Natural Gas Dehydration

Natural gas from the reservoir is usually saturated with water vapor (Ahmadi et al., 2021; Dalane et al., 2019; Mokhatab et al., 2018). Water present in natural gas can cause serious drawbacks including corrosion in transportation pipelines, flow line plugging, reduction in the heating value, loss of localized pressure, and reduction of line capacity (Chebbi et al., 2019; Dalane et al., 2019; Petropoulou et al., 2019).

The most common techniques employed for natural gas dehydration are absorption with a solvent, adsorption by a solid desiccant, and condensation by cooling (Dalane et al., 2019; Santos et al., 2021). In addition to the traditional method, membrane technology has been regarded as an attractive approach for the gas separation processes since it exhibits simplicity and high operation efficiency (Wang et al. (2021), He et al. (2020)).

The adsorption process can be performed on the desiccants such as molecular sieves, silica gel, and activated alumina (Sakheta & Zahid, 2018). Molecular sieves are the significant desiccant materials used for industrial dehydration units (Mesgarian et al., 2020). Because the solid desiccant, which is used for adsorption dehydration, can be regenerated, it is employed for adsorption-desorption cycles (Tay et al., 2016). The adsorption process is usually implemented in a packed bed tower.

[*] Corresponding Author.
Authors' Email Address: [1] **H. Amidzadeh** (hadi.amidzadeh8@gmail.com), [2] **E. Nemati Lay** (enemati@kashanu.ac.ir), [3] **A. Mohebbi** (alireza2010mh@gmail.com), [4] **E. Kamali** (erfan.kamali7396@gmail.com)

http://dx.doi.org/10.22108/GPJ.2022.133839.1120

The required gas dew point is an important criterion to determine which one of the methods is more appropriate. From the viewpoint of the economy, the adsorption-based process is more favorable for a very low dew point requirement (Esfandian & Garshasbi, 2020; Yu et al., 2021).

1.2. Simulation of Natural Gas Dehydration Process

The simulations of natural gas dehydration units in the literature were mainly (tri-ethylene glycol) TEG-based. The application of computer simulation to an industrial adsorption plant for natural gas dehydration has not received much attention in the literature.

Trueba et al. (2022) created effective operating procedures to control TEG consumption in the natural gas dehydration process. Excessive TEG circulation rates could decrease the reboiler temperature, decrease the amount of removed water from the natural gas, and increase TEG losses. So, the main part of their standard procedures consisted of adjusting the TEG circulation rate by automatic variation system according to the dehydration needs of the natural gas. They reported that their procedures could make operations more efficient.

Kong et al. (2020) extended the techno-economic assessment to evaluate three different configurations of DRIZO. With the use of recycling the flash vapor and the regenerator overhead into the dehydration process, they found the best configuration in which the highest TEG purity, the lowest TEG loss, and the lower water content in the dry gas product could be obtained.

Chebbi et al. (2019) optimized a TEG dehydration process using the Aspen HYSYS optimizer tool. Their optimization aimed to minimize the processing cost, which included both utilities and capital costs. TEG circulation rate, feed gas pressure and temperature, gas flow rate, stripping gas rate, and numbers of thetheoretical trays were considered important design parameters in their optimization. *Dalane et al. (2019)* considered a new subsea natural gas dehydration process with membrane and TEG. They optimized different process designs with the staging of the regeneration with inter-stage heating. Their optimization results revealed that the TEG flow rate was reduced by 55% and energy consumption by 37.8%. *Petropoulou et al. (2019)* optimized the dehydration process of natural gas with respect to energy saving. They investigated the effect of the operational parameters on the process. They found that the stripping gas rate and the duties in the reboiler and the cooler could be lowered by optimization. They reported that a significant reduction of the operating cost was achieved at optimized conditions. *Li et al. (2019)* evaluated two shale gas dehydration approaches economically. Besides, they presented the environmental assessment for the TEG-based dehydration approaches, namely, stripping gas and conventional dehydration process. They derived the data for utilities from Aspen Process Economic Analyzer. They revealed that the stripping gas performed better at fewer theoretical stages and from an economic point of view, the conventional process was found superior at a higher water content in the dry gas.

Sakheta and Zahid (2018) simulated the conventional dehydration process for natural gas with the dehydrating solvent of the TEG. They performed the simulation by using Aspen HYSYS. After validating the results against the plant data, they investigated the stripping gas design configuration by adding stripping gas to the reboiler or the bottom of the regeneration column. They showed that the energy requirement of the stripping gas configuration was about 50% lower than the conventional design. They reported that the performance of the stripping gas design was better because of the higher evaporation of water, higher concentration of TEG, and lower solvent recirculation.

With the use of a steady-state simulator (UniSim Design), *Neagu and Cursaru (2017)* simulated a natural gas dehydration plant. They investigated the effect of the hot stripping gas flow rate on the regenerated TEG concentration and dew point of the sale gases. They found that it was an effective way to improve the dehydration plant performance. *Santos et al. (2017)* investigated the dehydration of natural gas that contained high carbon dioxide content. They performed simulation with the adsorption simulator Adsim because the dynamic behavior of the adsorption and desorption could be properly predicted by Aspen Adsim software. They showed the water content of the saturated natural gas increased with rising CO_2 content in the gas. As a result, the service of the dehydration by molecular sieve and the adsorbent bed volume at a given high pressure was increased.

Torkmahalleh et al. (2016) put emphasis on the assigned thermodynamic models for the simulation of a TEG-based natural gas dehydration unit with the use of Aspen Plus. They employed combinations of thermodynamic models for the main unit operations instead of using one thermodynamic model for the entire unit. They reported that plant simulation results were improved by assigning the appropriate combination of the thermodynamic models.

El Mawgoud et al. (2015) simulated a dehydration gas plant using Aspen HYSYS program. To reduce the equipment cost and lower energy consumption, they investigated a modified scenario. In their proposed alternative, the air cooler was added in a glycol package to decrease the operating temperature of the contactor. *Ranjbar et al. (2015)* simulated a TEG dehydration unit in order to evaluate the effect of parameters including the glycol circulation rate

and the absorber's temperature on the water content of the dehydrated gas by a steady-state simulator, HYSYS. By implementing the optimized parameters, the water content of the dehydrated gas, glycol circulation rate, and reboiler duty were minimized. *Ghiasi et al. (2015)* considered two intelligent approaches to find the optimum stripping gas flow rate in natural gas dehydration unit. By using methods of neural networks and least squares, they estimated the TEG concentration as a function of stripping gas flow rate.

1.3. Natural Gas Hydrates

Natural gas hydrates are crystalline solids, consisting of both host and guest molecular species. Typical natural gas molecules such as methane, ethane, propane, and carbon dioxide become trapped in a water cage that is composed of hydrogen-bonded water molecules (Santos et al., 2021; Naeiji & Varaminian, 2018; Shuard et al., 2017). The formation of natural gas hydrates can cause serious problems such as reduction of pipeline capacity and blockage of equipment. *Ghaderi et al. (2021)* investigated the methane hydrate formation in presence of various inhibitors and modeled the kinetic parameters of the hydrate formation. *Chavoshi et al. (2018)* reviewed the empirical equations for hydrate formation presented in the literature. They evaluated the empirical correlations with the use of experimental data. For better evaluation, they divided the data into several groups including simple natural gas components and gas mixture similar to natural gas.

1.4. Objective

In spite of the research on the natural gas dehydration process (especially the TEG-based dehydration process), a proper study on the effect of dehydration unit performance on the hydrate formation temperature of the produced dehydrated gas is still lacking. This work addresses the gap by comparing the hydrate formation temperature of dry gas production for the simple dehydrator scheme and the proposed dehydration process with the pre-cooler. To the best of our knowledge, the literature review indicates that there is no information available about the effect of feed gas cooling before entering the adsorber on the hydrate formation temperature of the produced dry gas.

So, the primary objective of this paper is to improve the performance of a natural gas dehydration unit by installing a heat exchanger before the dehydrator to reduce the inlet temperature within Aspen Adsim simulation environment.

In doing so, we simulate the industrial molecular dehydration unit and design the heat exchanger to reduce the feed gas temperature. Then, we investigate the effect of temperature reduction on the temperature of hydrate formation and water content for the dry gas product.

On the other hand, the water content of the dehydrated gas is in close connection with the capacity of the molecular sieve to adsorb water. Molecular sieve capacity for the next cycle is strongly affected by heating time in the regeneration step. So, the effect of heating time in the regeneration step on the unit performance is discussed in the present study.

2. Process Description

The dry gas is produced in the molecular sieve process where the water in the wet gas adsorbs onto the bed of adsorbent (Carroll, 2020).

Fig. 1 shows a process flow diagram for a typical molecular sieve dehydration unit. The number of adsorber vessels changes with regard to the mode of operation and flow rate of the feed gas. As depicted in Fig. 1, the natural gas dryers can operate in the three parallel vessels dehydrating and one vessel on regeneration. Lower pressure drop and longer molecular sieve lifetime are the benefits of three-bed parallel operation (Mokhatab et al., 2018).

Figure 1

The mass transfer zone (MTZ) is a part of the bed in which the transference of a component (water) from the gas bulk to the solid surface occurs. The non-utilized zone is a section of the bed that is dry and not encountered with water. As the gas moves through the bed, the mass transfer zone moves until finally, the front edge of the MTZ reaches the end of the bed (Mokhatab et al., 2018). At this time, the entire bed is saturated with water and the adsorbent bed should be switched from the adsorption phase to the regeneration phase (Carroll, 2020).

The cycle of each dehydrator bed begins with adsorption, lasting for 480 minutes, and ends with regeneration. Heating and cooling are the main steps of regeneration. In the heating step, which lasts about 100 minutes, the gas (288℃) is passed upwards through the molecular sieve bed to remove the water and regenerate the dehydrator. After heating, the solid desiccant bed is cooled by the cold regeneration gas (57℃). The Aspen adsorption simulator (Aspen Adsim) is used to simulate the adsorption and regeneration processes (Fig. 2).

Figure 2

In order to simulate natural gas dehydration a reduced system comprising methane, ethane, CO_2, H_2O, and nitrogen is selected. The feedstock composition and the process parameters for the dehydration unit are tabulated in Table 1.

Table 1

The impact of high molecular weight

hydrocarbons on the adsorption is not considered, because: (i) more than 97% of the natural gas is composed of CH_4, C_2H_6, CO_2, H_2O, and N_2; (ii) since the adsorption model calibration is a major step, dependable equilibrium molecular sieve adsorption data for heavier hydrocarbons can be hard to find; (iii) heavier hydrocarbons have a limit interaction with molecular sieve caused by molecular size restrictions (Santos et al., 2017).

3. Effect of Feed Gas Temperature on the Product Gas from the Dehydrator

As depicted in Fig. 3, a reduction in the feed gas temperature can decrease the water content in the feed gas. The change in the gas water content can affect the performance of the dehydrator.

Figure 3

As illustrated in Fig. 4, the concentration of the adsorbate (water) in the solid adsorbent is a function of the temperature and the water concentration in the fluid phase. When the temperature increases, the adsorbent capacity falls.

Figure 4

4. Langmuir Adsorption Isotherm

In order to design the industrial adsorption processes and characterize the porous solids, adsorption isotherms are applied. Adsorption in microporous materials can be described by the Langmuir model. The Langmuir equation of adsorption can be easily applied to multicomponent adsorption processes. For the correlations of co-adsorption data of natural gas mixtures, co-adsorption isotherms corresponding to the dual site isotherm have proven to be beneficial (Keller & Staudt, 2005).

The dual-site Langmuir equation can describe real gas-solid adsorption systems. The favorable primary sites are filled first, followed by the less favorable secondary sites (Tang et al., 2016).

Dual-Site Langmuir is expressed by

$$W_i = \frac{IP_{1i} exp\left(\frac{IP_{2i}}{T_s}\right) P_i}{1+\sum_k \left(IP_{3k} exp\left(\frac{IP_{4k}}{T_s}\right) P_k\right)} + \frac{IP_{5i} exp\left(\frac{IP_{6i}}{T_s}\right) P_i}{1+\sum_k \left(IP_{7k} exp\left(\frac{IP_{8k}}{T_s}\right) P_k\right)}$$

The isotherm parameters for the Langmuir adsorption isotherm are tabulated in Table 2. Also, the parameters of 4Å Zeolite adsorbent are shown in Table 3.

Table 2
Table 3

5. Implementation of Pre-cooler

As mentioned before, the water content of wet gas is strongly affected by the temperature and increasing temperature reduces the natural gas water content. As a result, implementation of pre-cooler before the adsorber promotes the opportunity to adjust the inlet temperature. So, feed gas passes through pre-cooler heat exchanger before entering the dehydrators in order to transfer heat to the cold gas coming out from cold separator. The separator exists in the refinery near the dehydration unit.

5.1. Shell-and-Tube Heat Exchanger Design

The following equations are used to design the shell-and-tube heat exchanger (Kakaç et al., 2020)

5.2. Tube-Side Heat Transfer Coefficient, h_i

Gnielinski recommended the following correlation for the average Nusselt number

$$Nu_b = \frac{(f/2)(Re_b - 1000)(Pr_b)}{1+12.7(f/2)^{0.5}\left(Pr_b^{0.667}-1\right)} \quad (2)$$

$$A_{tp} = \frac{\pi d_i^2}{4}\frac{N_t}{2} \quad (3)$$

$$f = (1.58ln(Re_b) - 3.28)^{-2} \quad (4)$$

$$u_m = \frac{\dot{m}_t}{\rho_t A_{tp}} \quad (5)$$

$$h_i = \frac{Nu_b\, k}{d_i} \quad (6)$$

$$Re = \frac{\rho u_m d_i}{\mu} \quad (7)$$

5.3. Shell-Side Heat Transfer Coefficient, h_0

McAdams suggested the following correlation for the shell-side heat transfer coefficient

$$\frac{h_0 D_e}{k} = 0.36\left(\frac{D_e G_s}{\mu}\right)^{0.55}\left(\frac{c_p \mu}{k}\right)^{1/3}\left(\frac{\mu_b}{\mu_w}\right)^{0.14} \quad (8)$$

$$for\ 2\times 10^3 < Re_s = \frac{G_s D_e}{\mu} < 1\times 10^6 \quad (9)$$

$$D_e = \frac{4\left(P_T^2 - \pi d_0^2/4\right)}{\pi d_0} \quad (10)$$

$$G_s = \frac{\dot{m}}{A_s} \quad (11)$$

$$A_s = \frac{D_s C B}{P_T} \quad (12)$$

$$C = P_T - d_0 \quad (13)$$

The following equations are used for the

overall heat transfer coefficient, temperature difference and pressure drop

5.4. Overall Heat Transfer Coefficient, U_0

$$U_0 = \frac{1}{\frac{d_0}{d_i h_i} + \frac{d_0 \ln(d_0/d_i)}{2k} + \frac{1}{h_0}} \quad (14)$$

5.5. Log Mean Temperature Difference (LMTD) Method for Heat Exchanger

$$\Delta T_{lm} = \frac{(T_{h1} - T_{C2}) - (T_{h2} - T_{c1})}{ln\left(\frac{T_{h1} - T_{C2}}{T_{h2} - T_{C1}}\right)} \quad (14)$$

$$\Delta T_m = F \Delta T_{lm} \quad (15)$$

5.6. Shell-Side Pressure Drop

$$\Delta p_s = \frac{f G_s^2 (N_b + 1) D_S}{2 \rho D_e \varphi_s} \quad (16)$$

$$\varphi_s = \left(\frac{\mu_b}{\mu_w}\right)^{0.14} \quad (17)$$

$$N_b = {}^{L}/_{B} - 1 \quad (18)$$

$$f = exp(0.576 - 0.19 \ln Re_s) \quad (19)$$

5.7. Tube-Side Pressure Drop

$$\Delta p_s = \left(4f \frac{L N_p}{d_i} + 4N_p\right) \frac{\rho u_m^2}{2} \quad (20)$$

The Properties of feed gas and cold stream for the design of shell-and-tube heat exchanger are tabulated in Table. 4.

Table 4

6. Incomplete Regeneration

Insufficient regeneration time, low regeneration temperature, and a small gas flow rate will lead to a loss in adsorption capacity (Mokhatab et al., 2018).

For the gaseous compound at a given partial pressure and temperature, an equilibrium concentration of the adsorbate exists on the adsorbent surface. The level of gas dryness is a function of the regeneration parameters. A completely regenerated bed is in equilibrium with the regenerating gas. So, the performance of the regeneration is in connection with the concentration of water left on the adsorbent bed (Mokhatab et al., 2018)

7. The Results and Discussion

7.1. Model Validation

As shown in Tables. 5 and 6, the accuracy of the model was checked by comparing the obtained results with the plant data. Because the simulation results are in good agreement with the industrial plant data, the proposed simulation is reliable for the dehydration unit.

Table 5

Table 6

7.2. Design of Shell-and-Tube Heat Exchanger

The results of design parameters are shown in Tables. 7 and 8.

Table 7

Table 8

Inlet wet gas flows through the exchanger to exchange further heat with the cold stream. In the exchanger, the 15℃ reduction in the temperature of the feed gas is provided. Wet natural gas is precooled with the aid of the heat exchanger before directing it to the adsorber. To reduce the temperature from 48℃ to 33℃, the feed gas flows through the tube side of the heat exchanger.

7.3. Effect of Feed Gas Temperature on the Product Gas from the Dehydrator

The simulation results show that the water content of the product from the dehydrator decreases as the inlet feed gas temperature goes down, by considering the same feed composition (Table. 9).

Table 9

Fig. 5 illustrates that for the reduction of 15℃ in the feed temperature, about a 50% reduction in the product water content is attained. So, the pre-cooler can be used to make this drastic reduction in the water content of the gas product.

Figure 5

To maintain the wet gas at a suitable temperature before directing it to the dehydrator, a heat exchanger can be used to regulate the inlet zone temperature.

7.4. Comparison with Petropoulou et al. (2019), Sakheta and Zahid (2018) (Absorber Temperature in the TEG-based Natural Gas Dehydration Unit)

The absorber operating temperature is specified by the wet feed gas temperature. As the inlet feed gas temperature decreases, the solubility of water in the glycol increases; consequently, the water content of the dehydrated stream decreases (Figs. 6,7).

Figure 6

Figure 7

The results of our study for the reduction of

inlet feed temperature are entirely consistent with the reported results, but the effects of mentioned modifications on the hydrate formation temperature of the produced dehydrated gas have not been investigated yet.

Taking into consideration the values of dehydrated gas water content at the corresponding feed or contactor temperature of 33˚C (306K) in Figs. 5-7, it is revealed that although water content for the TEG-based dehydration unit (Figs. 6 and 7) reaches the values of about 40 to 50 ppm, water content for the adsorption unit (present study, Fig. 5) reaches the lower value of about 10 ppm. It is worth noting that the molecular sieves units are preferred when very low water content is necessary.

7.5. Insufficient Regeneration

As mentioned earlier, the performance of the regeneration is in connection with the concentration of water left on the adsorbent bed. In order to properly regenerate the adsorbents, the regeneration time should be monitored.

Fig. 8 shows a steeper decreasing trend for the H_2O holdup in the adsorbent bed before the heating time of 8000 seconds; after this time, Fig. 8 reaches a flatter section and doesn't change much.

Figure 8

As depicted in Fig. 9, a sharp rise can be seen in the total amount of removed water from the adsorbent bed during regeneration before the heating time of 8000 seconds; after this time, the amount of removed water shows small changes.

Figure 9

If the heating time in the regeneration step increased from 6000 seconds (current heating time) to 8000 seconds (proposed heating time), the reduction of 17.7% in the H_2O holdup in the adsorbent bed and the rise of 6.8% in the total amount of the removed water from the adsorbent bed during regeneration are achieved.

7.6. Comparison with Kong et al. (2019), Kong et al. (2020) (Regeneration Step in the TEG-based Natural Gas Dehydration Unit)

Because a conventional TEG-based dehydration process could not meet the water dew point specification (-25˚C) for pipeline-transported natural gas, Kong et al. (2019) developed a techno-economic framework to show that the water dew point requirement could only be met using a stripping gas dehydration process (Fig. 10). They reported the increasing trend for the TEG purity when the stripping gas flow rate went up. They revealed that the addition of stripping gas resulted in a reduction of the water partial pressure. So, the increase in stripping gas rate caused the increase of the lean TEG purity leading to a lower water content in the produced dry gas.

Figure 10

As illustrated in Fig. 11, when the stripping gas flow rate increases, after the flow rate of about 100 Nm^3h^{-1}, the TEG purity shows smaller changes and Fig. 11 reaches a flatter section. This trend is similar to our findings (Fig. 9). The total amount of the removed water from the dehydrating agent increases with the severity of the regeneration step.

Figure 11

7.7. Improvement in the Hydrate Formation Temperature of Product for the Proposed Dehydration Process Scheme with Pre-cooler

With the aid of the "Hydrate Formation Analysis of HYSYS Software," the temperature of hydrate formation is evaluated. We determine the hydrate formation temperature for the product of a simple dehydrator and the product of the proposed dehydration process scheme with a pre-cooler (Table 10).

Table 10

Figure 12

Fig. 12 demonstrates that hydrate formation temperature decreases efficiently for the adsorber with the proposed inlet exchanger.

The molecular sieve capacity is enhanced because the temperature is adjusted using directing the wet gas to the inlet heat exchanger. If the dehydrator performs under more convenient operating conditions, regulated temperature along the dehydrator leads to enhance the molecular sieve capacity significantly. Consequently, a considerable reduction in the hydrate formation temperature is obtained. Decreasing temperature improves the hydrate formation temperature because the water content of the inlet wet gas decreases as the temperature goes down (Fig. 12). Thus, appropriate cooling operation before entering the dryer is necessary to tune the temperature.

Hydrate formation can cause severe problems such as pipeline corrosion, process instrumentation plugging, high-pressure drop, and diminution in pipeline capacity. These problems are in close connection with the temperature of hydrate formation. On the other hand, Heat exchanger addition, which exchanges further heat with the cold stream, is an efficient approach to handling the extra heat and tuning the inlet hydrator temperature leading to producing the product with a lower hydrate formation temperature.

Table 11

In the proposed configuration, an appropriate cooling operation before entering the solid desiccant bed is applied to eliminate the extra heat by means of a shell and tube heat exchanger. Because of sufficient cooling operation under new operating conditions, the adsorbent capacity enhances and the temperature of

hydrate formation reduces significantly. So, the improvement of 12 to 26% in the temperature of hydrate formation for the proposed dehydration process with the pre-cooler in comparison with a simple dehydrator scheme is obtained (Table 11). In other words, the temperature of hydrate formation is improved by 6 to 7˚C depending on the pressure (Fig. 13).

Figure 13

8. Conclusions

The I dehydration unit aims to lower the dew point and water content of the natural gas. The main objective of this study is to improve the performance of a natural gas dehydration unit by introducing a heat exchanger before the dehydrator to reduce the inlet temperature. Aspen Adsim is employed in the simulation of the adsorption unit.

The temperature of wet natural gas is one of the most dominant factors affecting the adsorption process for the industrial dehydration unit. In the proposed dehydration configuration, the pre-cooler (shell and tube heat exchanger) has been appropriately designed to keep the wet natural gas and the corresponding water content varying within an acceptable limit and promote the opportunity to reduce the feed temperature effectively.

The product water content and the hydrate formation temperature for the proposed dehydration scheme are improved in comparison with the simple dehydration scheme because extra heat is removed in the new configuration. The proper temperature of the inlet dehydrator leads to a reduction in the temperature of hydrate formation by 12-26%, which is equivalent to 6.46-7.65˚C depending on pressure. This is mainly attributed to the dependence of adsorbent capacity on temperature. When the temperature increases, the concentration of water in the solid adsorbent falls.

The results show that the maximum effectiveness of this approach is achieved for 35.23 bar where the temperature of hydrate formation is decreased by 7.65˚C; it means that if the pressure of the pipeline conveying the dry natural gas product reaches 35.23 bar, hydrate begins to form in -41.25˚C instead of -33.60˚C. Blockage of equipment and reduction of pipeline capacity is the consequences of natural gas hydrates to downstream facilities. The lower temperature of hydrate formation is widely regarded as an important safety factor to avoid plugging of the flow line and increasing pressure drop. It is worthwhile to mention that if the immediate reduction in pressure is necessary for the flow line or equipment, the more convenient pressure for this operation can be calculated to hinder the formation of the hydrate.

Molecular sieve capacity for the next cycle is strongly affected by heating time in the regeneration step. If the heating time in the regeneration step is increased from 6000 to 8000 seconds (proposed heating time), H_2O holdup in the adsorbent bed and the total amount of the removed water from the adsorbent bed during regeneration are improved by 17.7% and 6.8%, respectively. The proper heating time of 8000s in the regeneration step enhances the capacity of the molecular sieve to adsorb water.

Nomenclature

A_i	Heat transfer area based on the inside surface area of tubes, m^2	Nu	Nusselt number
A_s	Crossflow area at or near shell centerline, m^2	Pr	Prandtl number
B	Baffle spacing, m	P_T	Pitch size, m
C	Clearance between the tubes, m	Q	Heat duty of heat exchanger, W
C_p	Specific heat at constant pressure, J/kg · K	Re_s	Shell-side Reynolds number
D_s	Shell inside diameter, m	T	Temperature, °C, K
d_o	Tube outside diameter, m	T_c	Cold fluid temperature, °C, K
d_i	Tube inside diameter, m	T_h	Hot fluid temperature, °C, K
F	Correction factor to LMTD for non-counter flow systems	T_w	Wall temperature, °C, K
f_i	Friction factor for flow across an ideal tube bank	U_c	Overall heat transfer coefficient for clean surface based on the outside tube area, $W/m^2 \cdot K$
G	Mass velocity, $kg/m^2 \cdot s$	u_m	Average velocity inside tubes, m/s
h_i	Tube-side heat transfer coefficient, $W/m^2 \cdot K$	Δp_{bi}	Pressure drop for one baffle compartment in crossflow, based on ideal tube bank, Pa
h_o	Shell-side heat transfer coefficient for the exchanger, $W/m^2 \cdot K$	Δp_s	Total shell-side pressure drop, Pa
k_s	Thermal	$\Delta T_{c,h}$	Cold and hot end

	conductivity of shell-side fluid, W/m · K		terminal temperature differences, °C, K
k_w	Thermal conductivity of tube wall, W/m · K	ΔT_{lm}	Log mean temperature differences, °C, K
L	Effective tube length of heat exchanger between tube sheets, m	ΔT_m	Effective or true mean temperature difference, °C, K
m_s	Shell-side mass flow rate, kg/s	μ_s	Shell fluid dynamic viscosity at average temperature, mPa/s
m_t	Tube-side mass flow rate, kg/s	μ_t	Tube fluid dynamic viscosity at average temperature, mPa/s
N_b	Number of baffles in the exchanger	ρ_s, ρ_t	Shell- or tube-side fluid density, respectively, at average temperature of each fluid, kg/m^3
N_c	Number of tube rows crossed between baffle tips of one baffle compartment	ϕ_s	Viscosity correction factor for shell-side fluids
N_t	Total number of tubes or total number of holes in tube sheet for U-tube bundle		

References

Ahmadi, M., Lindbråthen, A., Hillestad, M., & Deng, L. (2021). Subsea natural gas dehydration in a membrane contactor with turbulence promoter: An experimental and modeling study. *Chemical Engineering Journal*, *404*, 126535.

Carroll, J. (2020). *Natural gas hydrates: a guide for engineers*. Gulf Professional Publishing.

Chavoshi, S., Safamirzaei, M., & Pajoum Shariati, F. (2018). Evaluation of empirical correlations for predicting gas hydrate formation temperature. Gas Processing Journal, 6(2), 15-36.

Chebbi, R., Qasim, M., & Jabbar, N. A. (2019). Optimization of triethylene glycol dehydration of natural gas. *Energy Reports*, *5*, 723-732.

Dalane, K., Hillestad, M., & Deng, L. (2019). Subsea natural gas dehydration with membrane processes: Simulation and process optimization. *Chemical Engineering Research and Design*, *142*, 257-267.

El Mawgoud, H., Elshiekh, T., & Khalil, S. (2015). Process simulation for revamping of a dehydration gas plant. *Egyptian journal of petroleum*, *24*(4), 475-482.

Esfandian, H., & Garshasbi, V. (2020). Investigation of methane adsorption on molecular sieve zeolite (from natural materials). *Gas Processing Journal, 8*(2), 35-50.

Ghaderi Ardakani, M., Javanmardi, J., & Parvasi, P. (2021). A kinetic study of methane hydrate formation in the presence of ionic liquids and poly (N-vinylcaprolactam). *Gas Processing Journal, 9*(1), 43-50.

Ghiasi, M. M., Bahadori, A., Zendehboudi, S., & Chatzis, I. (2015). Rigorous models to optimise stripping gas rate in natural gas dehydration units. *Fuel*, *140*, 421-428.

GPSA. (2004). *Engineering Data Book* (twelfth ed.). Gas Processors Suppliers Association (GPSA).

He, X., Kumakiri, I., & Hillestad, M. (2020). Conceptual process design and simulation of membrane systems for integrated natural gas dehydration and sweetening. *Separation and Purification Technology, 247*, 116993.

Kakaç, S., Liu, H., & Pramuanjaroenkij, A. (2020). *Heat Exchangers: Selection, Rating, and Thermal Design* (Fourth ed.). CRC press.

Keller, J. U., & Staudt, R. (2005). *Gas adsorption equilibria: experimental methods and adsorptive isotherms*. Springer Science & Business Media.

Kong, Z. Y., Mahmoud, A., Liu, S., & Sunarso, J. (2019). Development of a techno-economic framework for natural gas dehydration via absorption using Tri-Ethylene Glycol: a comparative study on conventional and stripping gas dehydration processes. Journal of Chemical Technology & Biotechnology, 94(3), 955-963.

Kong, Z. Y., Wee, X. J. M., Mahmoud, A., Yu, A., Liu, S., & Sunarso, J. (2020). Development of a techno-economic framework for natural gas dehydration via absorption using tri-ethylene glycol: a comparative study between DRIZO and other dehydration processes. *South African Journal of Chemical Engineering*, *31*(1), 17-24.

Li, W., Zhuang, Y., Zhang, L., Liu, L., & Du, J. (2019). Economic evaluation and environmental assessment of shale gas dehydration process. Journal of Cleaner Production, 232, 487-498.

Mesgarian, R., Heydarinasab, A., Rashidi, A., & Zamani, Y. (2020). Adsorption and growth of water clusters on UiO-66 based nanoadsorbents: A systematic and comparative study on dehydration of natural gas. Separation and Purification Technology, 239, 116512.

Mokhatab, S., Poe, W. A., & Mak, J. Y. (2018). *Handbook of natural gas transmission and processing: principles and practices*. Gulf professional publishing.

Naeiji, P., & Varaminian, F. (2018). The Effect of Sodium and Chloride Salts on Tetrahydrofuran Hydrate Formation by Using a Differential Scanning Calorimetry. Gas Processing Journal, 6(2), 49-60.

Neagu, M., & Cursaru, D. L. (2017). Technical and economic evaluations of the triethylene glycol regeneration processes in natural gas dehydration plants. *Journal of Natural Gas Science and Engineering*, *37*, 327-340.

Petropoulou, E. G., Carollo, C., Pappa, G. D., Caputo, G., & Voutsas, E. C. (2019). Sensitivity analysis and process optimization of a natural gas dehydration unit using triethylene glycol. *Journal of Natural Gas Science and Engineering*, *71*, 102982.

Ranjbar, H., Ahmadi, H., Sheshdeh, R. K., & Ranjbar, H. (2015). Application of relative sensitivity function in parametric optimization of a tri-ethylene glycol dehydration plant. *Journal of Natural Gas Science and Engineering*, *25*, 39-45.

Sakheta, A., & Zahid, U. (2018). Process simulation of dehydration unit for the comparative analysis of natural gas processing and carbon capture application. *Chemical Engineering Research and Design*, *137*, 75-88.

Santos, K. M., Menezes, T. R., Oliveira, M. R., Silva, T. S., Santos, K. S., Barros, V. A., Melo, D. C., Ramos, A. L., Santana, C. C., & Franceschi, E. (2021). Natural gas dehydration by adsorption using MOFs and silicas: A review. *Separation and Purification Technology*, *276*, 119409.

Santos, M. G., Correia, L. M., de Medeiros, J. L., & Ofélia de Queiroz, F. A. (2017). Natural gas dehydration by molecular sieve in offshore plants: Impact of increasing carbon dioxide content. *Energy Conversion and Management*, *149*, 760-773.

Shuard, A. M., Mahmud, H. B., & King, A. J. (2017). An optimization approach to reduce the risk of hydrate plugging during gas-dominated restart operations. *Journal of Petroleum Science and Engineering*, *156*, 220-234.

Tang, X., Ripepi, N., Stadie, N. P., Yu, L., & Hall, M. R. (2016). A dual-site Langmuir equation for accurate estimation of high pressure deep shale gas resources. *Fuel*, *185*, 10-17.

Torkmahalleh, M. A., Magazova, G., Magazova, A., & Rad, S. J. H. (2016). Simulation of environmental impact of an existing natural gas dehydration plant using a combination of thermodynamic models. *Process Safety and Environmental Protection*, *104*, 38-47.

Trueba Jr, L., Gaston, T., Brackin, J., Miller, J., & You, B.-H. (2022). Effective strategies to reduce triethylene glycol consumption in natural gas processing plants. Case Studies in Chemical and Environmental Engineering, 5, 100196.

Wang, R., Zhang, Y., Xie, X., Song, Q., Liu, P., Liu, Y., & Zhang, X. (2021). Hydrogen-bonded polyamide 6/Zr-MOF mixed matrix membranes for efficient natural gas dehydration. Fuel, 285, 119161.

Yu, G., Xu, R., Wu, B., Liu, N., Chen, B., Dai, C., Lei, Z. (2021). Molecular thermodynamic and dynamic insights into gas dehydration with imidazolium–based ionic liquids. Chemical Engineering Journal, 416, 129168.

Figure Captions

Figure 1. Process flow diagram for a typical molecular sieve dehydration process (Mokhatab et al., 2018)

Figure 2. Dehydration process in the simulation environment

Figure 3. Water content of hydrocarbon gas (GPSA, 2004)

Figure 4. Typical water adsorption isotherms of a 4A molecular sieve (Mokhatab et al., 2018)

Figure 5. Effect of feed gas temperature on the product gas from the dehydrator

Figure 6. Effect of the contactor operating temperature on the dry gas water content (Petropoulou et al. (2019))

Figure 7. Effect of the contactor temperature on the water content for natural gas (Sakheta and Zahid (2018))

Figure 8. H_2O holdup in adsorbent bed at the end of heating time

Figure 9. Total amount of the removed water from the adsorbent bed during regeneration

Figure 10. Injection of stripping gas into the reboiler of the regeneration column (Kong et al. (2020))

Figure 11. TEG purity for the stripping gas dehydration process (Kong et al. (2019))

Figure 12. Comparison between a simple dehydrator and the dehydrator with a pre-cooler

Figure 13. Difference between gas hydrate formation temperature of simple dehydrator and dehydrator with pre-cooler as a function of pressure

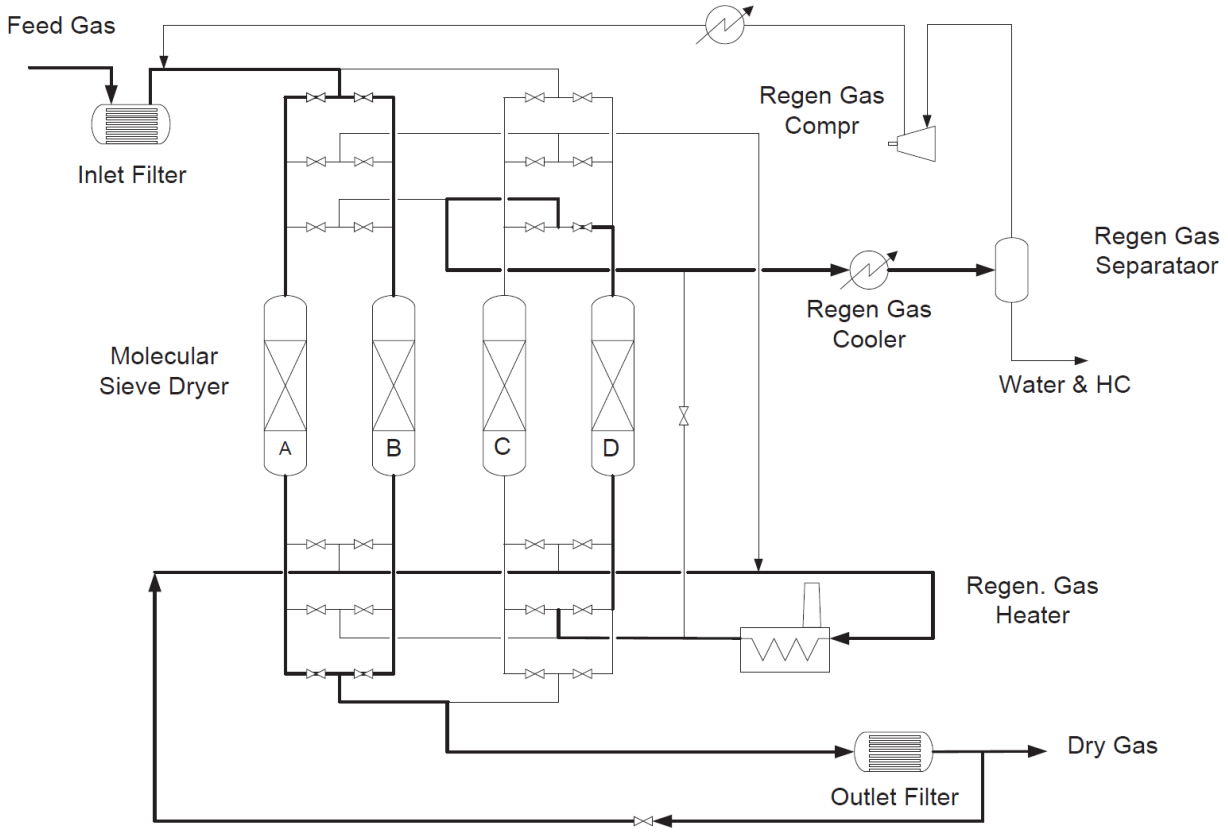

Figure 1. Process flow diagram for a typical molecular sieve dehydration process (Mokhatab et al., 2018)

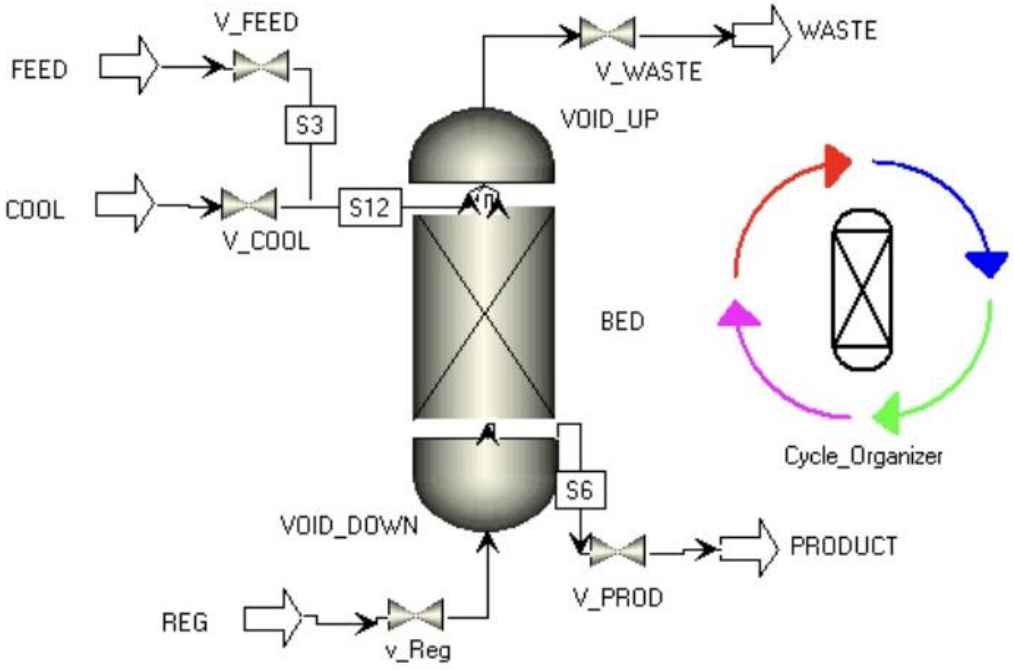

Figure 2. Dehydration process in the simulation environment

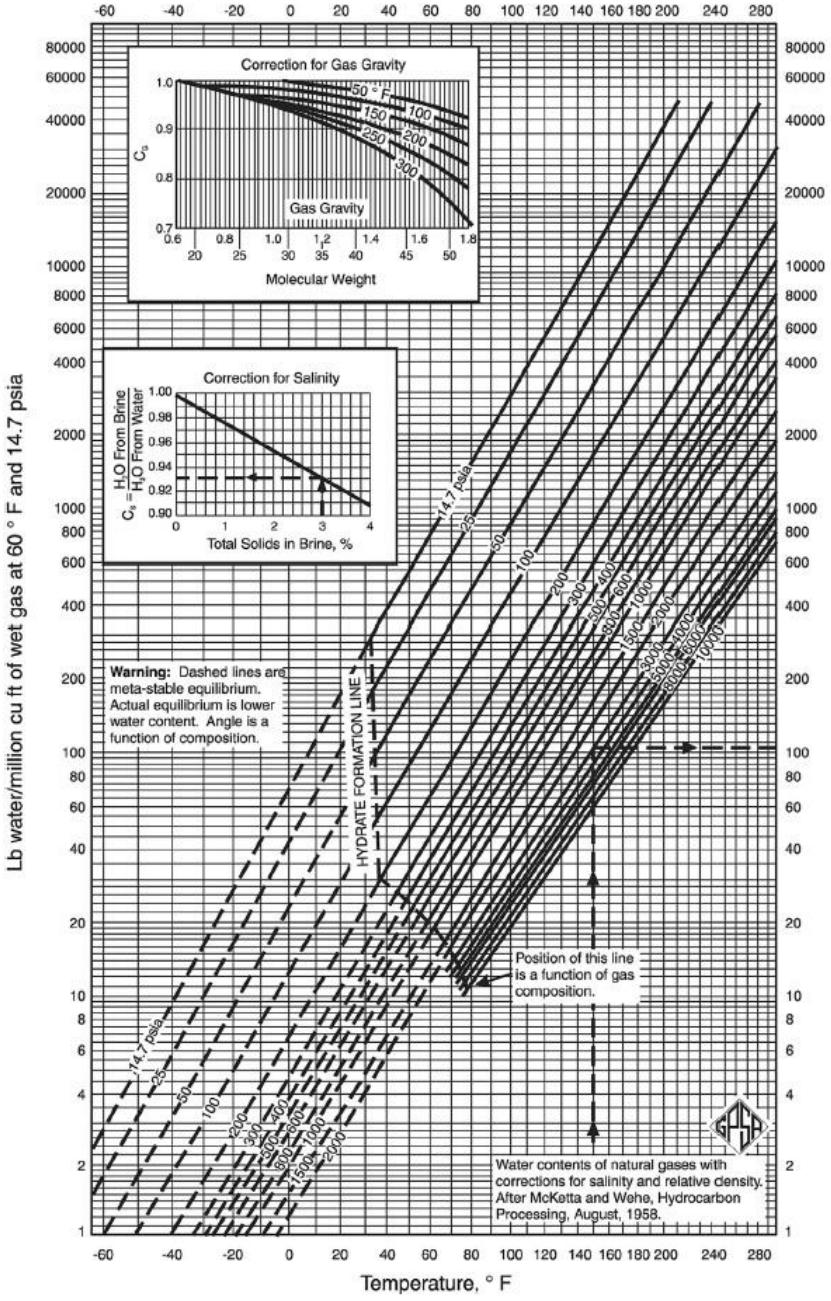

Figure 3. Water content of hydrocarbon gas (GPSA, 2004)

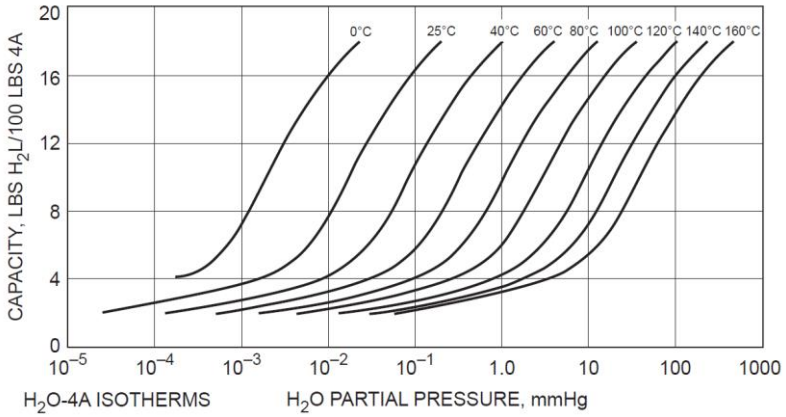

Figure 4. Typical water adsorption isotherms of a 4A molecular sieve (Mokhatab et al., 2018)

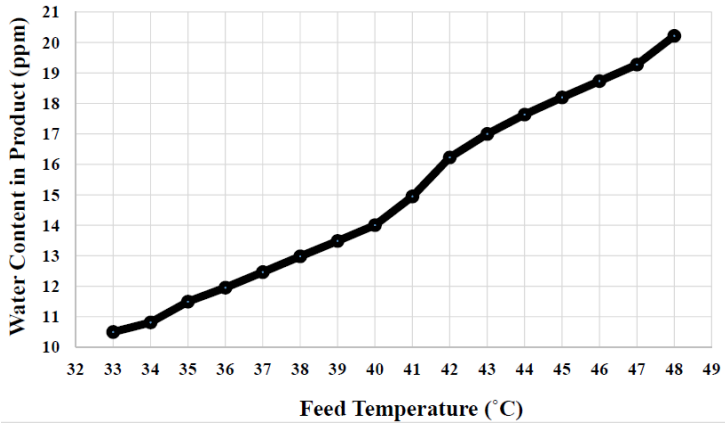

Figure 5. Effect of feed gas temperature on the product gas from the dehydrator

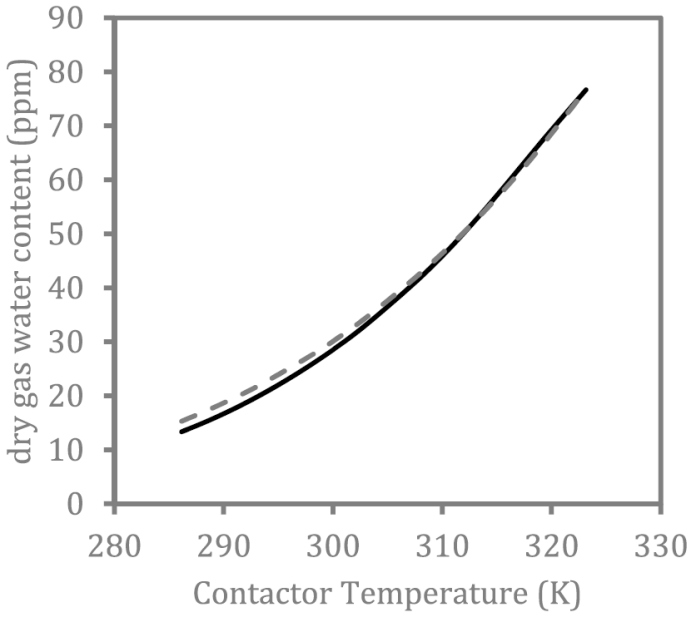

Figure 6. Effect of the contactor operating temperature on the dry gas water content (Petropoulou et al. (2019))

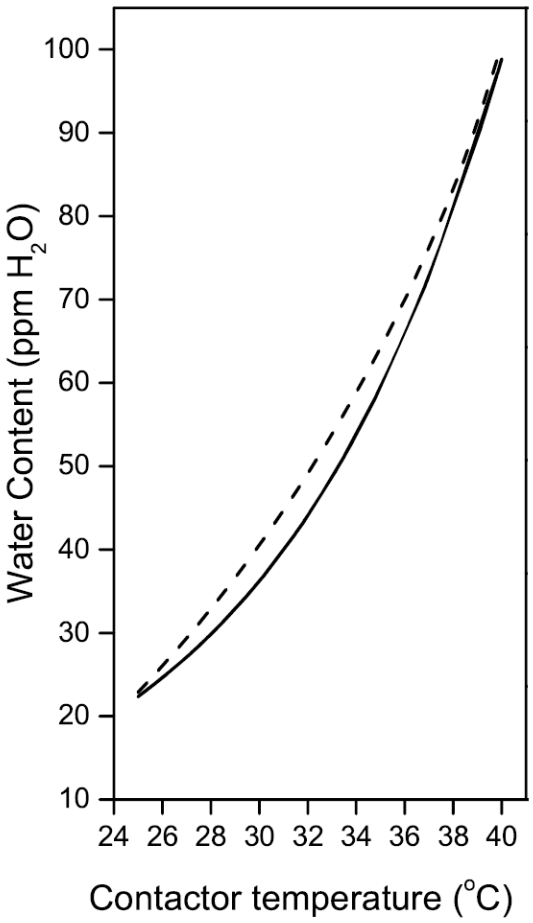

Figure 7. Effect of the contactor temperature on the water content for natural gas (Sakheta and Zahid (2018))

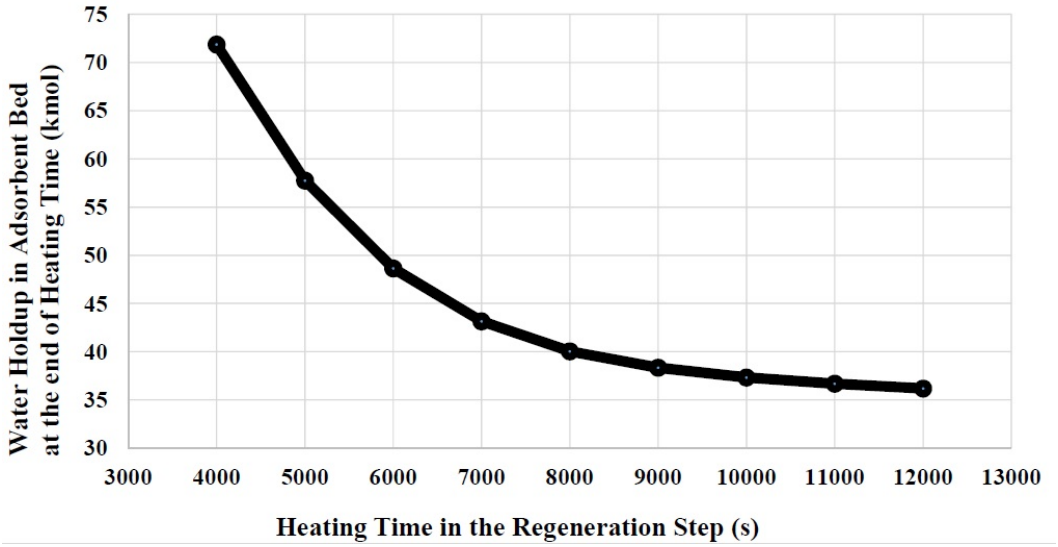

Figure 8. H2O holdup in adsorbent bed at the end of heating time

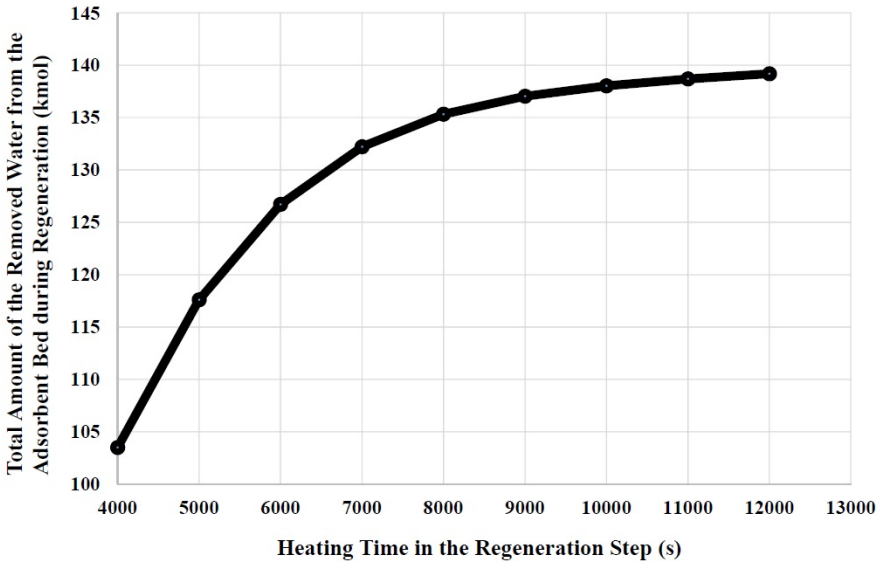

Figure 9. Total amount of the removed water from the adsorbent bed during regeneration

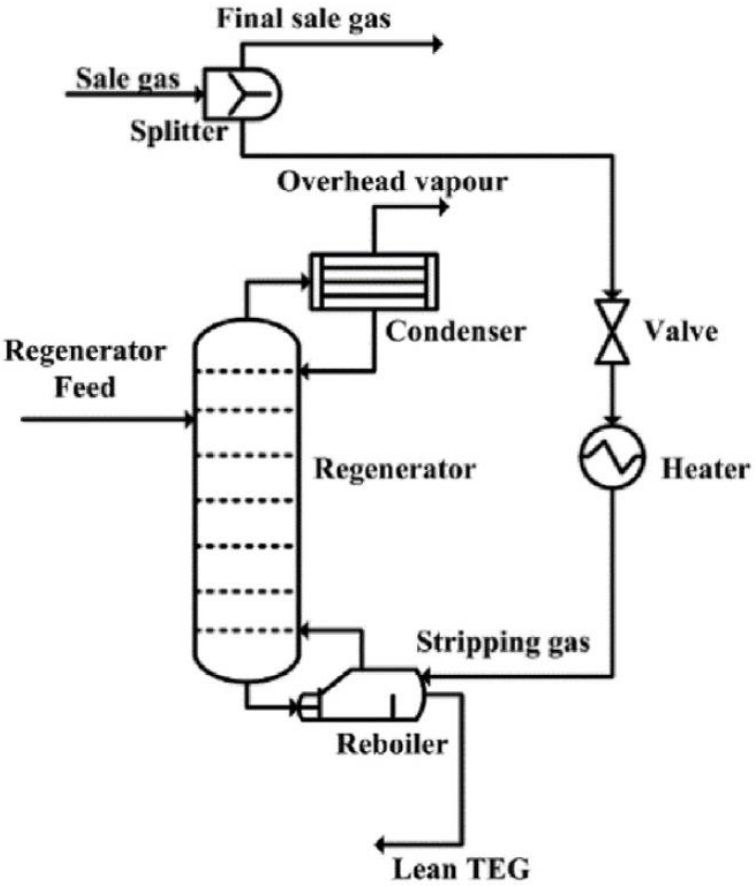

Figure 10. Injection of stripping gas into the reboiler of the regeneration column (Kong et al. (2020))

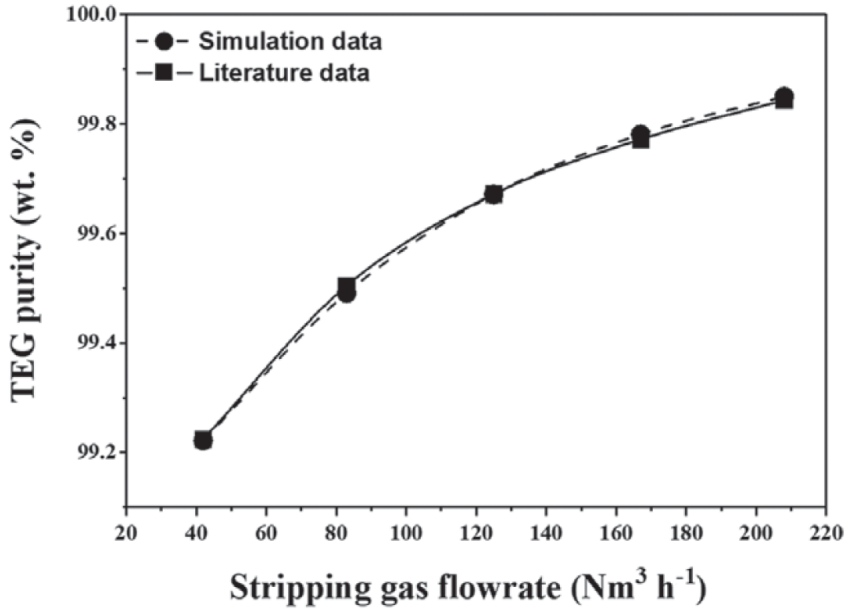

Figure 11. TEG purity for the stripping gas dehydration process (Kong et al. (2019))

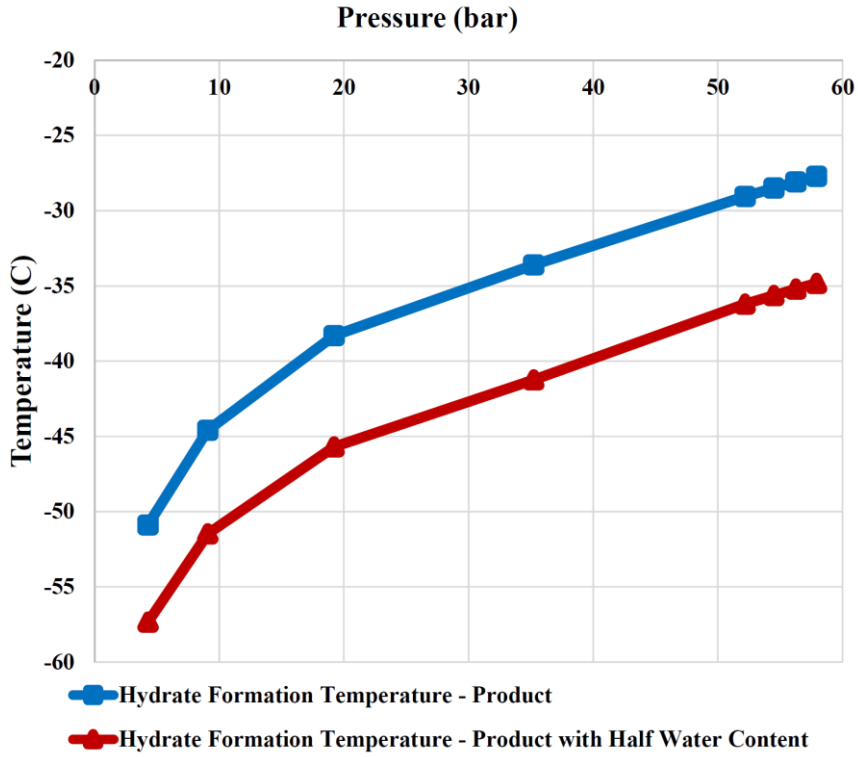

Figure 12. Comparison between a simple dehydrator and the dehydrator with a pre-cooler

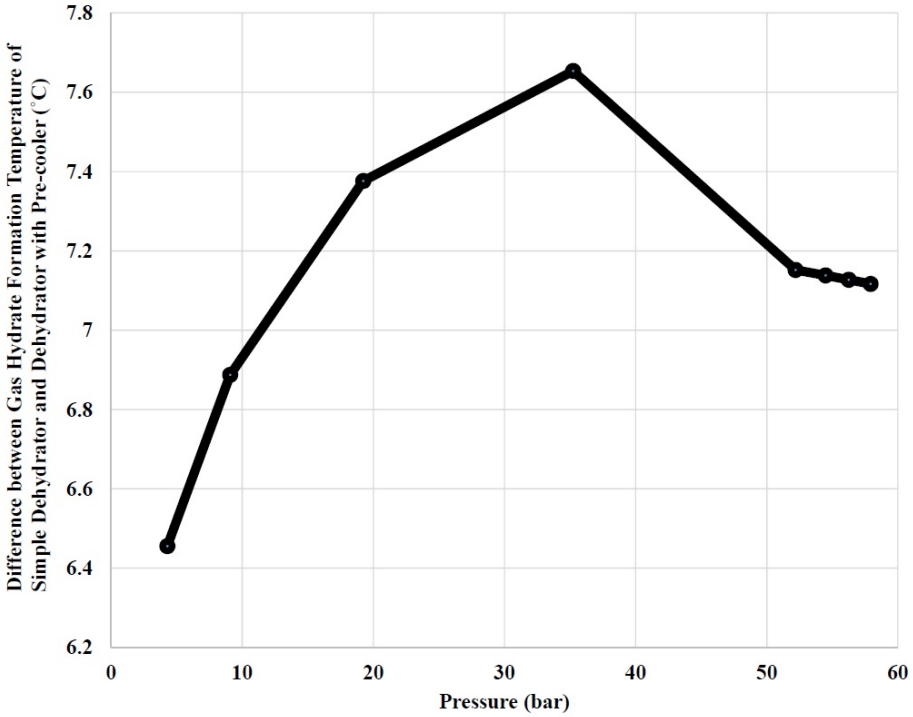

Figure 13. Difference between gas hydrate formation temperature of simple dehydrator and dehydrator with pre-cooler as a function of pressure

List of Tables

Table 1. The feedstock composition and operating conditions at the commercial dehydration unit in Iran

Unit loading	3104 [m^3h^{-1}]				
Feed Temperature	47 [°C]				
Pressure	90 [barg]				
Feed (mol. %)	Methane (CH_4)	Ethane (C_2H_6)	Carbon Dioxide (CO_2)	Water (H_2O)	Nitrogen (N_2)
Data Set 1	87.58	7.98	1.55	0.09	2.80
Data Set 2	87.70	8.30	1.57	0.08	2.35
Data Set 3	86.75	8.76	1.66	0.09	2.74

Table 2. Isotherm parameter for the Langmuir adsorption isotherm

Isotherm parameter (IP)	Values for				
	C_1	C_2	CO_2	H_2O	N_2
IP(1)	0	3.37E-08	1.46E-05	1.81E-07	3.00E-06
IP(2)	0	3757	2862	6138	1460
IP(3)	0	1.41E-05	0.00867	2.18E-05	7.93E-04
IP(4)	0	3757	2862	6138	1460
IP(5)	0	0	4.74E-06	1.24E-04	0
IP(6)	0	0	2111	5420	0
IP(7)	0	0	0.00312	0.0757	0
IP(8)	0	0	2111	5420	0

Table 3. Parameters of 4Å zeolite adsorbent

Parameter	Symbol	Value	Unit
Height of adsorbent layer	H_b	6.0	m
Internal diameter of adsorbent layer	D_b	3.0	m
Inter-particle voidage	E_i	0.34	m^3 void/m^3 bed
Intra-particle voidage	E_p	0.28	m^3 void/m^3 bed
Bulk solid density of adsorbent	RHOs	746.0	kg/m^3
Adsorbent particle radius	R_p	3.0	mm
Specific surface area of adsorbent	a_p	660.0	1/m
Adsorbent specific heat capacity	C_{ps}	1.07	kJ/kgK

Table 4. Properties of feed gas and cold stream

Property	Feed stream (tube side)	Cold stream (shell side)
ρ (kg/m^3)	72.59	57.71
C_p (j/kg K)	2113	2081
μ $(kg/m.s)*10^5$	1.447	1.335
k $(w/m.k)*10^2$	4.302	3.919
Pr	0.711	0.709

Table 5. Comparison between the simulation results and experimental data

Component (mol. %)		Methane (CH4)	Ethane (C2H6)	Carbon Dioxide (CO2)	Water (H2O)	Nitrogen (N2)
Data Set 1	Experiment (mol. %)	0.8782	0.0804	0.01560	1.25E-05	0.0257
	Simulation (mol. %)	0.8717	0.0811	0.0159	1.59E-05	0.0310
Data Set 2	Experiment (mol. %)	0.8777	0.0828	0.01580	1.38E-05	0.0236
	Simulation (mol. %)	0.8711	0.0831	0.0165	1.03E-05	0.0290
Data Set 3	Experiment (mol. %)	0.8815	0.0742	0.0154	1.38E-05	0.0288
	Simulation (mol. %)	0.8718	0.0811	0.0159	1.60E-05	0.0310

Table 6. Mean absolute relative error for component

Component	Mean Absolute Relative Error
C_1	0.0086
C_2	0.0407
CO_2	0.0319
H_2O	0.2283
N_2	0.1986

Table 7. Results of design parameters for tube-side and shell-side

	Tube-Side	Shell-Side
ΔT (°C)	15	15.23
h (w/m² k)	3234	1088
ΔP (Pa)	96016	122511

Table 8. Results of design parameters for heat exchanger

ΔT_{lm} (°C)	12.88
UA (w/k)	45228
L (m)	4.50

Table 9. Effect of feed gas temperature on the product gas from the dehydrator

Feed Temperature (Inlet Temperature) (°C)	Water Mol Fraction in Product (ppm)
33	10.49
34	10.81
35	11.49
36	11.95
37	12.46
38	12.98
39	13.48
40	14.00
41	14.94
42	16.22
43	16.99
44	17.63
45	18.19
46	18.73
47	19.27
48	20.21

Table 10. Results of Hydrate Formation Analysis of HYSYS software for the product of simple dehydrator and product of the proposed dehydration process scheme with a pre-cooler

Pressure (bar)	Hydrate Formation Temperature (°C)	
	Product	Product with Half Water Content (Due to 15°C Reduction in Feed Temperature)
4.290	-50.88	-57.34
9.082	-44.60	-51.48
19.23	-38.31	-45.69
35.23	-33.60	-41.25
52.19	-29.05	-36.21
54.49	-28.50	-35.64
56.26	-28.09	-35.21
56.78	-27.97	-35.09
57.92	-27.71	-34.83

Table 11. Comparison between simple dehydrator (current process) and the dehydrator with pre-cooler (proposed Process)

Pressure (bar)	Hydrate Formation Temperature (°C)		ΔT (°C)	Percent of Improvement
	Simple Dehydrator (Current Process)	Dehydrator with Pre-cooler (Proposed Process)		
4.290	-50.88	-57.34	6.46	12.70
9.082	-44.60	-51.48	6.88	15.43
19.23	-38.31	-45.69	7.38	19.26
35.23	-33.60	-41.25	7.65	22.77
52.19	-29.05	-36.21	7.61	24.65
54.49	-28.50	-35.64	7.14	25.05
56.26	-28.09	-35.21	7.12	25.35
56.78	-27.97	-35.09	7.12	25.46
57.92	-27.71	-34.83	7.12	25.69